Experimental study of pH effect on uranium (U^{VI}) particle formation and transport through quartz sand in alkaline 0.1 M sodium chloride solutions

Matthew Edward Kirby (Conceptualization) (Data curation) (Formal analysis) (Investigation) (Methodology) (Project administration) (Resources) (Software) (Supervision) (Validation) (Visualization) (Writing - original draft), Jonathan Stuart Watson (Data curation) (Formal analysis) (Validation) (Writing - original draft) (Writing - review and editing) (Writing - review and editing), Jens Najorka (Data curation) (Formal analysis) (Validation) (Writing - original draft), Janice Pauline Louvane Kenney (Formal analysis) (Writing - original draft) (Writing - review and editing) (Writing - review and editing), Samuel Krevor (Conceptualization) (Funding acquisition) (Investigation) (Project administration) (Resources) (Software) (Supervision) (Validation) (Visualization) (Writing - original draft) (Writing - review and editing), Dominik Jakob Weiss (Conceptualization) (Data curation) (Formal analysis) (Funding acquisition) (Investigation) (Methodology) (Project administration) (Resources) (Software) (Supervision) (Validation) (Visualization) (Writing - original draft) (Writing - review and editing)

PII: S0927-7757(19)31373-1

DOI: https://doi.org/10.1016/j.colsurfa.2019.124375

Reference: COLSUA 124375

To appear in: *Colloids and Surfaces A: Physicochemical and Engineering Aspects*

Received Date: 28 October 2019

Revised Date: 18 December 2019

Accepted Date: 18 December 2019

Please cite this article as: Kirby ME, Watson JS, Najorka J, Louvane Kenney JP, Krevor S, Weiss DJ, Experimental study of pH effect on uranium (U^{VI}) particle formation and transport through quartz sand in alkaline 0.1 M sodium chloride solutions, *Colloids and Surfaces A: Physicochemical and Engineering Aspects* (2020), doi: https://doi.org/10.1016/j.colsurfa.2019.124375

Experimental study of pH effect on uranium (U^{VI}) particle formation and transport through quartz sand in alkaline 0.1 M sodium chloride solutions

Matthew Edward Kirby[1], Jonathan Stuart Watson[1], Jens Najorka[2], Janice Pauline Louvane Kenney[1,3], Samuel Krevor[1], Dominik Jakob Weiss[1,4]

[1]Earth Science and Engineering, Imperial College London, United Kingdom
[2]Imaging and Analysis Centre, Natural History Museum, United Kingdom
[3]Earth and Planetary Sciences, MacEwan University, Edmonton, Alberta, Canada
[4] School of Earth, Energy and Environmental Sciences, Stanford University, United States

Graphical abstract

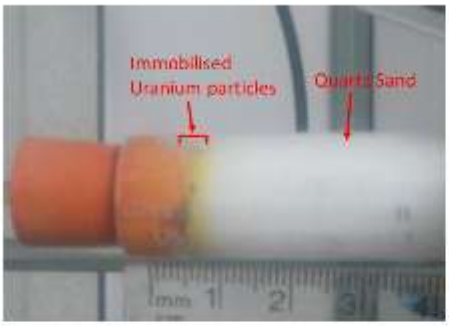

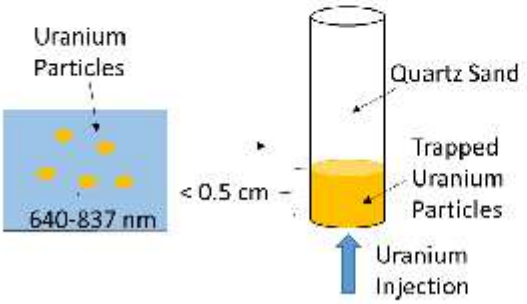

Abstract

A thorough understanding of the aqueous uranium VI (U^{VI}) chemistry in alkaline, sodium containing solutions is imperative to address a wide range of critical challenges in environmental engineering, including nuclear waste management. The aim of the present study was to characterise experimentally in more detail the control of pH on the removal of U^{VI} from aqueous alkaline solutions through particle formation and on subsequent transport through porous media. We conducted first static batch experiments in the pH range between 10.5 and 12.5 containing 10 ppm U^{VI} in 0.1 M NaCl solutions and examined the particles formed using filtration, dynamic light scattering, transition electron microscopy and X-ray powder diffraction. We found that at pH 10.5 and 11.5, between 75 and 96% of U^{VI} was removed from the solutions as clarkeite and studtite over a period of 48 hours, forming particles with hydrodynamic diameters of 640 ± 111 nm and 837 ± 142 nm, respectively and representing aggregates of 10's nm sized crystals randomly orientated. At pH 12.5, the formation of particles >0.2 µm became insignificant and no U^{VI} was removed from solution. The mobility of U^{VI} in these solutions was further studied using column experiments through quartz sand. We found that at pH 10.5 and 11.5, U^{VI} containing particles were immobilised near the column inlet, likely due physical immobilisation of the particles (particle straining). At pH 12.5, however, U^{VI} quantitatively eluted from the columns in the filter fraction <0.2 µm. The findings of our study reinforce a strong control of solution pH on particle size and U removal in alkaline solutions and subsequently on mobility of U through quartz porous media.

.

Keywords: pH; uranium; particle; formation; alkaline; NaCl

Introduction

Uranium (U) is a toxic element that threatens groundwater quality if mobilised from a solid-phase source such as geological disposal facilities [1-3] or during fluid-rock interactions in natural geological settings [4-6]. Of particular and immediate concern worldwide is radioactive material stored temporarily in grout-free aqueous solutions where the pH is adjusted with sodium hydroxide to prevent containers and materials in the solution from dissolving [7, 8]. At Hanford in the United States of America, for example, high level liquid radioactive waste collected from reprocessing Pu for nuclear weapons is stored in carbon-steel tanks. These tanks contain 5.2 to 13.4 M Na and 31 ppm U in solutions of pH 13 [7, 9, 10]. At Sellafield in the United Kingdom, spent fuel rods are stored in storage ponds at pH > 10 [8].

The formation of uranium precipitates in alkaline solutions is well documented. For example, U^{VI} was observed to precipitate as a U^{VI}-calcium carbonate particle from Hanford groundwater when the solution pH was raised to above 10.5 [10] and the solutions contained sediments which acted as nucleation points. U^{VI} was also observed to precipitate from sodium containing solutions (0.01 M NaCl and 0.05 M $NaClO_4$) at pH between 9 and 11 [11, 12]. Recent studies in our group explored the removal of U^{VI} in 0.1 M NaCl solutions between pH 2 and 12 in contact with quartz, sandstone and volcanic rocks representing possible bedrocks for nuclear waste storage and with bacteria [13, 14]. When the concentration of U^{VI} was 10 ppm, U^{VI} precipitated as Na containing minerals with 20 nm crystals aggregated to particles with diameter ≥0.45 micron at pH ≥10. The ≥0.45 μm diameter U^{VI} aggregates no longer formed above pH 12, demonstrating the importance of distinct pH windows on the control of uranium removal from solutions. The size of U^{VI} precipitates was also characterised in a synthetic cement leachate at pH 13.1 [15]. The U^{VI} precipitates were 2 nm diameter crystals consisting of a clarkeite-type phase containing Ca^{2+}, K^+ and Na^+. These crystals were shown to aggregate into 10 to 60 nm diameter colloids in solutions with U^{VI} ranging between 1 and 10 ppm, and into ≥ 0.22 μm diameter particulates, when 60 ppm U^{VI} was present in the cement leachate. Further studies also determined the zeta potential of calcium uranate (CaU_2O_7) in 0.01 M NaCl solutions

as -22.2 mV [16] and of Na-boltwoodite ($Na[(UO_2)(SiO_3OH)]\bullet H_2O$) in 0.1 M $NaClO_4$ solutions above pH 10 as -46 mV [17].

Despite the interest in understanding the formation and stability of U^{VI} particles in alkaline solutions [18-20], investigations identifying accurately the range where pH changes lead to precipitation and the implications of this pH window on subsequent mobility are missing, in particular for sodium containing solutions. The mobility of U^{VI} in these alkaline solutions is best assessed using column experiments where the solution/solid ratio is more realistic of geological environments. A recent study assessed the elution profiles of 0.48 ppm U^{VI} in 1 mM $NaClO_4$ at pH 11 through unsaturated quartz sand [21] and found between 72-82% of the U^{VI} was eluted from the column with precipitates observed in the samples collected at the column outlet. The mobility of U^{VI} was also tested in 0.1 M NaOH and 1.0 M $NaNO_3$ at pH 13 using groundwater equilibrated Hanford sediment columns by injecting 0.35 mg of U^{VI} into the columns, followed by an injection of U^{VI} free groundwater [9]. U^{VI} precipitated near the column inlet and the authors attributed this to the formation of Na-boltwoodite ($Na(UO_2)(SiO_3OH)\bullet 2H_2O$). When the pH decreased below 9.5, the U^{VI} mineral dissolved, and further uranium from the pre-contaminated Hanford sediment was mobilised.

The aim of the present study was to explore systematically the pH control and the mechanisms of U^{VI} removal through particle formation in sodium containing aqueous solutions in the range between pH 10.5 and 12.5 and during the subsequent transport through porous silica media. Previous work identified this pH window as critical with respect to amount of U^{VI} being removed from alkaline solutions [13-15, 22]. To this end, we characterised particle formation (temporal evolution, particle size, surface charge, mineralogy) using static batch experiments with solutions containing 10 ppm of U^{VI} in 0.1 M NaCl at pH 10.5, 11.5 and 12.5 and tested the elution behaviour of these solutions through well characterised glass columns packed with porous quartz sand media (grain size, pore throat size, pore size, surface charge).

Materials and Methods

2.1 Chemicals and materials

Chemicals were analytical grade or better and solutions were prepared with 15 MΩ.cm de-ionised water (Merck Millipore). NaOH pellets and distilled 6 M HCl were used to prepare 1 M NaOH and HCl solutions used for pH adjustments. 4.5 M HNO_3 solutions were prepared from a distilled 15.5M nitric acid bulk solution and used to dissolve the U^{VI} mineral to characterise the quartz sand column retention profiles. A 1000 mg/L U PerkinElmer Pure Plus standard solution was used to prepare U^{VI} solutions. NaBr (Sigma-Aldrich) was used as a non-reactive tracer. Na_2CO_3 and NaOH (Sigma-Aldrich) was used to prepare the anion eluent for Ion Chromatography. A 997±4 mg/L Si standard (Tracecert, Fluka) was used to prepare Si standards. Washed and calcined quartz fine granular sand, diameter ≥40% 0.2-0.8 mm (Merck Millipore) was used as the porous media in the columns. The sand was cleaned with a series of acid and base washes detailed elsewhere [23]. For analysing the zeta potential with DLS, the sand was crushed until its diameter was approximately 1 µm, and the cleaning procedure was then repeated.

2.2. Analytical Techniques

2.2.1. Determinations of pH and dissolved CO_2

The solution pH was measured using a Metrohm pH meter calibrated at three (pH 4, 7 and 10) or four points (pH 4, 7, 10, 13). The three-point calibrated meter was checked with a pH 13 glycine buffer (Sigma Aldrich). This was within ±0.04 pH units of the pH 13 buffer and had a precision of ±0.015.

Dissolved $\Sigma[CO_2]$ was determined using an Orion CO_2 ion sensing electrode. The electrode was calibrated using at least three points between 0.1 and 5 mM $NaHCO_3$. A buffer solution (0.5 ml) was added to samples to reduce pH to ca. 4.8 so all aqueous carbonate species were converted to aqueous CO_2.

2.2.2. Elemental analysis of U, Si and Br

U^{VI} concentrations were determined using an Agilent Technologies, 7900 ICP-MS. One ml aliquots from batch or column experiments were diluted 8 to 10 times using 2(v/v)% HNO_3. An external calibration was carried out at the start and end of sample measurements, and a Bi internal standard was used to correct for drift. Typical detection limit was 0.16 ppb. A 1 ppm U standard prepared was measured multiple times showing a reproducibility of ±2% (1 S.D.).

Silicon concentrations were determined using a Thermo Scientific iCap 6500 duo view ICP-AES. The limit of quantification was 50 ppb. Repeat analysis of an in-house standard gave a typical RSD% of 1. The bias relative to the in-house standard estimated from nine repeat analysis was 6.5%.

Bromide concentrations were determined using a Metrohm 930 Compact IC Flex ion chromatograph with a Metrostep supp 16 150/4.0 6.1031.420 anion chromatography column for the pH 12.5 column experiment and with ICP-MS for the pH 10.5 and 11.5 column experiments.

2.2.3. Dynamic Light Scattering (DLS)

Dynamic Light Scattering (DLS) was used to analyse the size distribution and the zeta potential (Z_p) of the particles. The hydrodynamic diameter was calculated from the translational diffusion co-efficient of the particles and the Z_p was calculated from the electrophoretic mobility [24, 25]. The U^{VI} precipitates and quartz sand showed a broad size distribution with a polydispersity index of 1.00, therefore the size distribution by intensity was discussed rather than the Z-average.

Triplicate samples were prepared and measured 48 hours after production. The U^{VI} solutions were prepared in 15 ml test tubes and left stationary so that it reproduced the conditions of the static batch experiments. Solutions containing the crushed quartz were prepared at a quartz concentration of 10 ppm and these were placed on a rotary device for 48 hours. The samples were shaken by hand immediately before analysis and 1 ml aliquot was placed in a cuvette. Each sample was measured three times using a

ZEN5600 Malvern Zetasizer Nano ZSP with detection range of 0.3 nm to 10 µm. The number of scans for each size distribution measurement was at least 10. The precision based on 1 S.D was typically ±127 nm. A 12.8˚ scattering angle was used for the quartz samples and U^{VI} samples at pH 10.5 and pH 11.5 and a 173˚ was used to measure the samples at pH 12.5. Blank samples derived count rates were less than 1% of the quartz and U^{VI} samples. The precision of the Z_p was typically within ±2.5 mV based on 1 S.D.

2.2.4. Transmission Electron Microscopy (TEM)

The particles were left to settle at the bottom of the test tube and the solution was pipetted out until approximately 1.5 ml remained. The sample was then shaken and a drop was pipetted onto a copper stack with carbon membrane. The pH 10.5 samples were analysed with a Jeol JEM 2001-plus TEM, while a Jeol JEM 2100F was used to analyse the pH 11.5 samples. Energy dispersive x-ray spectroscopy (EDS) was used to confirm the precipitates contained U^{VI}. The analyses were carried out with an operating voltage of 200 kV. The detection limit for each element was 1 wt%.

2.2.5. X-Ray Powder Diffraction (XRD)

The quartz sand was analysed for several hours using an ENRAF NONIUS FR590 Diffractometer, with a Cu source operating at 35 mA and 40 kV. The incident X-ray beam was confined to pure Cu Kα1 radiation using a Germanium (111) monochromator in combination with horizontal slits set at 0.25 mm. Measurements were carried out in reflection using a fixed beam-sample-detector geometry. The diffracted X-rays were collected with an INEL 120º curved position sensitive detector. The angular linearity of the detector was calibrated with silicon and silver behenate standards and a 2θ linearization was carried out using a least-squares cubic spline function. The XRD pattern (Figure S1) was compared to reference pattern 00-046-1045 [26], confirming that only the quartz mineral phase was present. Additional measurements were performed without a sample to evaluate the contribution of the zero-background holder, which showed no peaks. XRD analysis was also performed to identify the U^{VI} bearing phase for

particles initially formed in solutions containing 10 mg/L U^{VI} and 0.1 M NaCl at pH 10.5 and 11.5. The particles could settle at the bottom of the test tube before being pipetted onto a glass slide and left at room temperature until the sample had dried. 15 MΩ.cm water was periodically applied to the dried U^{VI} bearing mineral and removed with paper, to remove excess salt. The dried precipitates were scraped onto a sapphire substrate zero-background holder and analysed overnight using the same operational parameters as employed for the quartz sand. The diffraction patterns were compared to datasets in the PDF4 ICDD 2014 database.

2.2.6. X-Ray Computed Tomography (X-ray CT)

Three dimensional images of a representative quartz sand column were acquired using X-Ray Computed Tomography (X-ray CT). The X-ray CT scans were taken with a Zeiss Xradia Versa 500 system. The X-ray source was operated with the anode voltage at 50 kV and power at 4 W. The X-rays were polychromatic and had a maximum energy of 50 keV. No source filter was used, and the projections were collected on a CCD camera with a pixel count of 2048 × 2048. A 4x objective was used to achieve a resolution of 3.5 µm per voxel; 2200 projections were taken as the sample was rotated through 180° around an axis perpendicular to the X-ray beam. The exposure length was determined such that 9000 counts were obtained through the centre of the projection. The grain, pore, and pore throat size distributions were extracted from the CT images. Approximations for grain diameter was determined by extracting grain volume using Avizo 9.3 [27] followed by calculating the spherical radius of the particles. Pore and pore throat radius were extracted using a previously developed pore network model in our labs [28].

2.3. Experimental designs of static batch and column experiments

2.3.1. Static batch experiments

Static batch experiments were conducted in duplicate for up to seven days following published procedures [29, 30]. The 200 ml solutions with 10 ppm U^{VI} and 0.1 M NaCl were brought to pH 10.5, 11.5 and 12.5. An approximately 180 ml solution containing NaCl was adjusted to the appropriate pH so that a 5 ml representative blank could be collected at each pH value. 42 µM U^{VI} (10 ppm) was added to the solution by diluting the 1000 ppm U^{VI} standard solution. The pH was re-adjusted to 11.5 and volume increased to 195 ml. The pH was measured and adjusted throughout the experiment with 1 M NaOH and 1 M HCl. The pH was measured on collection of a sample, excluding the column experiments where the pH was checked every hour. The solutions were shaken by hand immediately before sample collection to ensure the precipitates were suspended. The 5 ml samples were filtered through 0.2, 0.45, 0.8 and 1 µm nylon filter membranes (Whatman) and analysed for U^{VI}.

2.3.2. Column experiments

Column experiments were conducted at pH 10.5, 11.5 and 12.5 with 0.1 M NaCl and 10 ppm U^{VI} in duplicate following published procedures [23, 31]. For the pH 12.5 experiment, two glass chromatography columns (Chemglass CG-119-01) with 1.3 cm internal diameter (ID), and a 40-60 µm porous glass frit at the base of the column, were packed with approximately 40 g of quartz sand (sand column length = 19 cm). A glass frit and approximately 0.04 g of glass wool were placed at the top of the columns and sealed with a rubber stopper modified to contain an outlet tube. Water was pumped upwards through the column at 0.5±0.1 ml/min using a Cole-Palmer L/S Masterflex peristaltic pump (model 77240-00) until the column was saturated. For the experiments at pH 10.5 and 11.5, the glass frit at the column inlet was replaced with a steel mesh [23, 31]. The glass chromatography columns were wet packed to minimise air

entrapment. The water height was kept at least 1 cm above the sand level and the column was tapped gently to prevent layering.

The pore volume (PV) was determined gravimetrically. The porosity (ϕ) was calculated by dividing the PV by the total volume of the packed columns. The total volume of the column was calculated geometrically using $h\pi r^2$ where h and r is the height and radius of the column, respectively. The dry bulk density (ρ_b) was calculated by dividing the mass of the dry sand by the total volume of the sand column. The Darcy velocity (q) and average linear velocity (v) were then calculated.

The columns were equilibrated with a U^{VI} free solution at the desired pH overnight. Approximately 12 pore volumes of the U^{VI} solution was injected into the columns during the pH 12.5 experiments, and 6 pore volumes of U^{VI} were injected during the pH 10.5 and pH 11.5 experiments. The solution was then switched to one without U^{VI}. The solution was pumped upwards through the columns to minimise air entrapment, prevent flow due to gravity, and to ensure an even spread of the solution across the cross-sectional area of the column.

During the pH 10.5 and 11.5 column experiments, three samples were collected from the U^{VI} containing inlet solution and filtered with a 0.2, 0.45 and 1 µm Whatman nylon filter membrane at the start and end of U^{VI} injection to determine the amount of U^{VI} which had precipitated before injection into the column. Several outlet samples were filtered with 0.2 µm Whatman nylon filter membranes to determine whether any precipitates were leaving the column. Several samples were collected from the column outlet during initial column equilibrium and during U^{VI} injection. These samples were analysed for [Si]. A separate column experiment was conducted at pH 12.5 to determine the dissolved [Si].

At the end of the pH 10.5 and 11.5 column experiments, the sand was removed using a spatula in 1.5 cm increments and placed in 10 ml of 4.5 M HNO_3 to dissolve the U^{VI} to determine the retention profile of the U^{VI} precipitates. These were placed on a rotary device for at least 48 hours. 1 ml of the solution was diluted to 2% (v/v) $HNO_3$and then analysed for U^{VI}. The quartz sand was dried at 60 ˚C so that the mass of

U^{VI} could be normalised against the mass of the quartz sand. The U^{VI} mass balance was typically ca. 90% when considering the mass of U^{VI} injected into the column, the mass of U^{VI} retained in column and the mass of U^{VI} eluted from column.

2.4. Calculation of geochemical species present in solution

Uranium speciation and saturation indices were predicted between pH 9 and 13 using PHREEQC [32] in conjunction with the Andra Thermochimie (SIT) database [33]. The constant input conditions used for all pH values was 10 ppm U^{VI} and 0.1 M NaCl. The solution was equilibrated with O_2 assuming its atmospheric partial pressure is 0.2, (log(0.2) = -0.7). The $\Sigma[CO_2]$ was added as CO_3^{2-} and the software automatically splits the CO_2 into $CO_{2(aq)}$, HCO_3^- and CO_3^{2-} depending on pH. The average $\Sigma[CO_2]$ from the column experiments (220 µM) was used for all pH values. [Si] used was 1.44, 2.38 and 0.95 ppm at pH 10.5, 11.5 and 12.5 respectively. The solution was charge balanced by adding Na^+, representing the addition of NaOH to the experiments. The stability data for sodium boltwoodite and sodium weeksite were added into the SIT database using values given by the NEA database [34].

Results and Discussion

3.1 U^{VI} speciation calculations for solutions

Calculated concentrations of the aqueous U^{VI} species and calculated saturation indices for U^{VI} minerals which could potentially precipitate from solution are shown in Figure 1. The speciation model indicates that aqueous mononuclear uranyl hydroxide species ($[UO_2(OH)_3]^-$ and $[UO_2(OH)_4]^{2-}$) are the major aqueous species across the pH range of interest, with approximately 20% of U^{VI} present in a carbonate containing species ($[(UO_2)_2(CO_3)(OH)_3]^-$ or $[(UO_2)(CO_3)_3]^{4-}$) at pH 10.5. The carbonate complexes, however, are negligible at pH 11.5 and 12.5. The doubly charged $[UO_2(OH)_4]^{2-}$ dominates at pH >12.

The saturation indices suggest a variety of sodium and silicon containing uranium minerals are oversaturated and could potentially precipitate from solution. These are sodium compreignacite ($Na_2(UO_2)_6O_4(OH)_6•7H_2O$), sodium diuranate ($Na_2U_2O_7$), clarkeite ($Na(UO_2)O(OH)$), and sodium boltwoodite ($Na(H_3O)(UO_2)(SiO_4)•H_2O$). The latter mineral can be ignored during the batch experiments because the Si concentration was measured at the outlet of the quartz sand columns and is a result of the dissolution of the quartz sand. The saturation index of most minerals decreases as the pH increases (sodium compreignacite, sodium boltwoodite) with sodium compreignacite crossing the line from saturated to unsaturated between pH 12 and 12.5.

3.2. Temporal evolution of U^{VI} particle formation during batch experiments at pH 10.5, 11.5 and 12.5

Figure 2 shows the temporal evolution of U^{VI} particle formation during the batch experiments at pH 10.5, 11.5 and 12.5 derived from the ratio of [U^{VI}] in filtrates (C) over the [U^{VI}] in initial solution (C_0). During the first set of experiments, 5 ml samples were collected and filtered through 0.2, 0.45, 0.8 and 1 µm diameter filter membranes over a one week period (168 hours). The same amount of U^{VI} was removed by all filter sizes during these experiments. Therefore, during the second repeat, the samples were only filtered through a 0.2 µm filter membrane.

Batch experiments at pH 10.5: The results of the pH 10.5 batch experiments (Figure 2a) show that U^{VI} forming particles were removed rapidly from solution. Approximately 15 and 27% of the [U^{VI}] remained in the filtrate after two days for the two batch experiments. After one week, approximately 25 and 11% of U^{VI} remained in the filtrate in the first and second batch experiments, respectively.

Batch experiments at pH 11.5: During the batch experiment conducted at pH 11.5 (Figure 2b), after 48 hours, 11% and 4% of U^{VI} were remaining in the solution following filtration through filter membranes with diameters ranging between 0.2 and 1 µm. U^{VI} forming particles were removed from the solution more rapidly in the second batch experiment. The results show similar amounts of U^{VI} removal using four

filter membrane sizes indicating that the size fraction of the precipitates formed at pH 11.5 were ≥ 1 µm in diameter.

Batch experiments at pH 12.5: During the pH 12.5 batch experiments, U^{VI} quantitatively passed through the filter membranes showing that U^{VI} did not form particles with diameters > 0.2 micron (Figure 2c). This confirmed the findings of previous experiments reported by our group [14]. The U^{VI} could be present as the dissolved species $[UO_2(OH)_4]^{2-}$ (Figure 2a). The thermodynamic equilibrium calculations give a saturation indices at pH 12.5 of 4.59 and 5.38 for clarkeite and sodium diuranate (Figure 1) suggesting the solution could be oversaturated with these two minerals, respectively, and could precipitate from solution. Therefore, U^{VI} could be present as precipitates with diameter <0.2 µm. This would be in line with work studying 10 ppm U^{VI} aqueous cement leachates at pH 13.1 which found 60 nm colloids of a clarkeite type mineral containing Na, K and Ca was precipitating from solution [15].

3.3. Physico-chemical properties of the U^{VI} particles

3.3.1. Particle size and zeta potential

To obtain better insight into the size and the zeta potential of the particles formed in solution, samples containing 10 ppm U^{VI} and 0.1 M NaCl were collected after 48 hours in triplicate at pH 10.5 and 11.5 and in duplicate at pH 12.5 and prepared for subsequent analysis.

These solutions were first analysed using DLS. The results for the size and Z_p measurements are provided in Table 2. Histograms of size distribution by intensity at pH 10.5 and 11.5 can be found in the supplementary information (Figure S1 and S2). The DLS measurements indicated that at approximately pH 10.3, the diameters of the particles were typically between 459 to 955 nm, with average diameter of 640 ± 111 nm. The Z_p of the particles at pH 10.34 were -22.4 ± 1.04 mV. The U^{VI} particles detected at pH 11.4 had a greater average diameter of 837 ± 142 nm with particle diameter occurring typically between

530-1300 nm. The Z_p at pH 11.5 were -20.9 ± 0.19 mV, less negative than at pH 10.5. No particles were detected in the 10 ppm U^{VI} solutions at pH 12.43. (The detection limit of the DLS was 200 nm).

Transmission electron microscopy (TEM) combined with energy dispersive spectroscopy (EDS) was used to gain better insight into the morphology of the particles. Figure 3 shows TEM images of U^{VI} precipitates collected from a 42 µM U^{VI}, 0.1M NaCl pH 10.5 solution and taken during this study (panels B,C and E) and during our previous study [14]. Panel A is at 8k magnification. Panel B, C and D were imaged at 400k magnification and represent location A, B and C circled on panel A. Panel E is a Fast Fourier Transform (FFT) image of the precipitate. The greater magnification (400k) reveals clearly that the particles were aggregations of much smaller crystals (10's nm diameter) with a flaky morphology. Additional TEM pictures taken of U^{VI} precipitates prepared from pH 11.5 solutions and presented in Figure S5 showed a diameter of ≥1.2 µm in the X-direction and ≥ 0.8 µm in the Y-direction and a square shape with diameter of approximately 0.5 µm.

The hydrodynamic particle diameter calculated using DLS for the particles formed at pH 10.5 (459 to 955 nm) and at pH 11.5 (530 to 1300 nm) were within the diameters observed in the TEM images at pH 10.5 (375 to ≥1250 nm) and pH 11.5 (500 to ≥1200 nm). The TEM images show these particles were non-spheroidal, indicating they can be removed by the filter membranes which are larger than the pores average spheroidal diameter. The hydrodynamic diameter of the particles can lead to an under predicted particle diameter due to the non-spheroidal nature of the particles compared to the TEM images.

3.3.2. U^{VI} mineral identification using X-ray diffraction.

To determine the mineralogy of the particles, particles formed in the 10 ppm U^{VI}, 0.1 M NaCl solutions at pH 10.5 and 11.5 were dried, washed with water to remove NaCl, and analysed using X-ray diffraction. The XRD patterns of the solid phase formed in solutions initially at pH 10.5 and 11.5 are presented in Figure 4a-c against U^{VI} phase standard patterns. At pH 11.5, the standard with the greatest match is sodium diuranate ($Na_2U_2O_7$) with a slight deficiency of Na ($Na_6U_7O_{24,}$ (i.e. $Na_{1.72}U_2O_{6.86}$) PDF4 ICDD

reference pattern [5-446]) [35]. However, several low intensity peaks in the experimental patterns are missing from the reference pattern (36.5° and 40.5° 2θ) which suggests multiple mineral phases are present. This could be sodium diuranate ($Na_2U_2O_7$ PDF4 ICDD reference pattern [43-347]) [36] combined with studtite (UO_4•$4H_2O$, PDF4 ICDD reference pattern [49-1821]) [37] whose standard patterns are shown as black and orange circles in Figure 4b respectively, or alternatively clarkeite ($NaUO_2O(OH)$•H_2O, reference pattern [50-1586]) [38] combined with studtite shown by the black and orange circles in Figure 4c, respectively. A combination of sodium diuranate and studtite, or clarkeite and studtite can account for the unidentified peaks at 36.5° and 40.5° 2θ. Identifying whether the mineral is clarkeite or sodium diuranate is challenging using XRD as the diffractograms are very similar [18, 38]. PHREEQC can determine which minerals would likely precipitate from solution by equilibrating the solution with all the minerals in Figure 1b at critical saturation (SI = 0). This leads to all the U^{VI} precipitating from solution as clarkeite. Therefore, combining the XRD data with the thermodynamic modelling suggest clarkeite and studtite are precipitating from solution.

The peaks at pH 10.5 have shifted to a lower angle compared to the pH 11.5 sample, a new peak is observed at 19°, and another disappears at 36.5°. No reference patterns in the PDF4 ICDD 2014 database matched the pH 10.5 experimental pattern, but due to its similarity to the pH 11.5 experimental pattern, and the standard patterns presented in Figure 4, the U^{VI} precipitate at pH 10.5 is likely a similar mineral phase.

The broad peaks in XRD pattern of precipitates collected from solution of pH 10.5 and 11.5 (Figure 4) suggest that the precipitate is made up of crystals with diameter less than 100 nm, in agreement with the fast Fourier transform image and magnified TEM image presented in Figure 3 and discussed in detail previously.

3.4. U^{VI} transport through quartz sand in 0.1 M NaCl solutions between pH 10.5 and 12.5

3.4.1 Characterisation of quartz sand and column

Details of the quartz sand characterisation are given in the supplementary information. In brief, the quartz grains were angular with a bimodal grain size distribution (Figure S4). The two dominant grain diameters were at 20 µm and between 60 to 240 µm. The sand had a median grain size (d_{50}) of 120 µm. The pore and pore throat diameters were usually between 10 to 34 µm and 4 to 20 µm respectively, in agreement with typical literature values for the diameter of sand grains observed in the CT images [39]. The average Z_p of triplicate independent samples were -40.8 ± 1.19 mV, -42.0 ± 2.16 mV and -34.4 ± 1.96 for pH 10.5, 11.5 and 12.5 respectively. Z_p measurements of 1-5 µm diameter quartz sand particles at pH 9 in 0.1 M NaCl provided similar results of approximately -38 mV [40].

The physical properties of the column experiments are given in Table 2 and the pH and [Si] data are given in Table 3. The flow rate (Q) used in the column experiments were between 0.45-0.53 ml/min. The Darcy velocity (q) calculated from the flow rate was between 0.34-0.40 cm/min, in line with the velocity used by Bradford and co-workers [31] (0.10 cm/min) and Xu and co-workers [23] (0.31 cm/min) during similar particle transport experiments.

The results of the non-reactive tracer tests using Br for the experiments are provided in Figure 5a-c. The tailing during breakthrough of a Br free solution indicated the expected non-ideal behaviour [41]. The CT images (Figure S4) highlight the system was heterogeneous, and the non-ideal Br elution curves supported this. The increased pore volume (PV) and ϕ at pH 10.5 and 11.5 were caused by changing to a wet packing method which reduce the amount of air entrapment. Trapped air in the pH 12.5 experiment did not appear to effect transport as the behaviour of the Br tracer is similar for all the column experiments.

3.4.2 Elution profiles of U^{VI} solutions at pH 10.5, 11.5 and 12.5

Solutions containing 10 ppm U^{VI} in 0.1 M NaCl solutions at pH 10.5, 11.5 and 12.5 were injected into the quartz sand packed columns after being left in the reservoir for two days to allow for the particle formation (Figure 2). Two column experiments were conducted for each of the three pH values studied (10.5, 11.5 and 12.5) and the results are shown in Figure 5. The amount of U^{VI} in the filtrate at the start of injection ranged between 55-60 and 35-46% for the solutions at pH 10.5 and between 2.3 and 2.6% for the solutions at pH 11.5. Table 4 gives the details of the % of U^{VI} determined in the filtrates of inlet solutions at the end and at the start and in the outlets.

Elution profile at pH 10.5: At pH 10.5, approximately 64 and 37% of U^{VI} were eluted from the columns during the first and second column experiments, respectively (Figure 5a). The quantity of U^{VI} eluting from the column during the second experiment (37%) was the same amount of U^{VI} passing through the filter membranes at the start (Table 4, 35-46%) indicating that the U^{VI} containing particles were quantitatively immobilised in the column. Slightly more U^{VI} eluted from the column (64%) than remained in the filtrate for the first column experiment (55-60%). When the outlet solution was filtered through 0.2 micron filter membranes, a further 19% and 16% of U^{VI} was removed from solution, reducing the amount of U^{VI} in the filtrate from 64% and 37% to 45% and 21% for the first and second column experiments, respectively. This indicates that some of the U^{VI} was eluted from the sand columns as precipitates with diameter ≥0.2 microns while the remaining 45% and 21% U^{VI} were transported in the truly dissolved phase or as precipitates with diameter <0.2 microns. This implies that the amount of U^{VI} which precipitated from solution increased during transport through the quartz sand. It is unlikely that a U^{VI} silicate mineral were precipitating from solution because the thermodynamic modelling indicates only clarkeite precipitates from solution (Figure 1). It is also unlikely that the quartz surface was acting as nucleation points leading to the formation of a surface precipitate [42] because previous studies using the same chemical conditions as this study observed no removal of U^{VI} precipitates by quartz sand [14]. However, enhanced U^{VI}

precipitation could have been the result of solution agitation during transport as increased mixing would have caused the U^{VI} mineral forming ions to collide with increasing probability, enhancing the precipitation reaction rate [43]. When the injection solutions were switched to a pH 10.5 and 0.1 M NaCl solution without U^{VI}, approximately 7% and 15% of U^{VI} were eluted from the two columns. The percentage of U^{VI} in the outlet solutions after filtering through 0.2 µm filter membranes (column 1 = 6%, column 2 = 12%) was indeed approximately the same as the non-filtered outlet solution showing that U^{VI} was not being eluted as ≥0.2 µm diameter particles. This indicates that the U^{VI} precipitates which were immobilised during U^{VI} injection were slowly being re-entrained, either by dissolving or disaggregating as precipitates with diameter < 0.2 µm diameter.

Elution profile at pH 11.5: Less than 1% of U^{VI} was eluted from the columns during the injection of the pH 11.5 solution onto the columns (Figure 5b). Filtering the outlet solution with 0.2 µm filter membranes showed similar amounts of U^{VI} in the filtrate and unfiltered outlet samples (Table 4) indicating the mobile fraction did not contain particles ≥ 0.2 µm. The amount of U^{VI} remaining in the inlet solution after filtration through 0.2, 0.45 and 1 µm filter membranes at the beginning of injection ranged between 2.3 and 3.3% for both column experiments. These results indicate that virtually all U^{VI} had precipitated from solution, and the U^{VI} particles were immobilised within the column. When the injected solution was changed to a solution without U^{VI}, the elution of U^{VI} from the column remained approximately the same (1.4- 1.6%). Filtering the outlet solution with 0.2 µm filter membranes did not reduce the quantity of U^{VI} within the filtrate compared to the unfiltered solutions, indicating U^{VI} was not leaving the column as a ≥ 0.2 µm diameter particles.

Elution profile at pH 12.5: At pH 12.5 (Figure 5c) the elution curves showed a quantitative breakthrough for U^{VI} within 3.09 and 3.13 PV for columns 1 and 2 respectively, like that of the non-reactive tracer. This indicates that U^{VI} was highly mobile when particles did not form.

3.4.3. Retention profiles of U^{VI} at pH 10.5, 11.5 and 12.5

The retention profiles of the column experiments at pH 10.5 (Figure 6a) show that increased quantities of the U^{VI} particles were immobilised near the column outlet. 7.3 µg U^{VI}/g sand and 48.5 µg U^{VI}/g sand were immobilised within the top 1.5 cm of both columns. Below an average depth of 6.75 cm, the quantity of U^{VI} immobilised decreased in the remaining column lengths from 2.81 to 1.69 µg U^{VI}/g sand in column 1 and from 2.90 to 2.40 µg U^{VI}/g sand in column 2. The retention profiles for the pH 11.5 experiments (Figure 6b) showed that virtually all U^{VI} is immobilised within the first 1.5 cm of the column, near the solution inlet.

3.6. Possible mechanisms leading to U^{VI} immobilisation in quartz sand

The particles containing U^{VI} can be immobilised by two processes, i.e. due to attractive electrostatic and Van der Waals forces acting between the particles and the quartz sand and due to physical properties of the particles and quartz sand. The experimental results presented here suggest physical immobilisation.

The particles can be immobilised physically in the column because of the physical properties of the porous media (pore and pore throat diameter) and the particles (diameter). If the particles are bigger than the pores or pore throats then the particles will be trapped, a process known as particle straining [23, 31, 44]. An empirical relationship of this straining process has been observed in glass beads and quartz sand columns, which relates the mean diameter of the travelling particles (d_p), and median grain size of the porous media (d_{50}). This relationship shows that significant immobilisation by straining occurs when d_p/d_{50} is >0.005-0.008 [23, 31]. The median grain size (d_{50}) for the quartz sand is 120 µm while the average diameter of the U^{VI} particles is 640 ± 111 nm and 837 ± 114 nm at pH 10.5 and pH 11.5 respectively. The calculated d_p/d_{50} using these diameters is 0.0053 and 0.0070, within the range observed for significant straining [23, 31]. The d_p/d_{50} is further increased when considering the smaller size range observed in the

bimodal distribution of the sand (Figure S4a). Assuming d_{50} is 20 µm d_p/d_{50} increases to 0.032 and 0.042 for the precipitates formed at pH 10.5 and pH 11.5 respectively. The X-ray CT imaging indicates the pore and pore throat diameters are dominant between 10 to 34 µm and 4 to 20 µm, respectively (Figure S4b-c), in agreement with literature values for the diameter of sand grains observed here [39]. These pores and pore throats are larger than the U^{VI} precipitates diameter, however, the resolution of the CT imaging is 3.5 µm which means pore throats with smaller diameters which are associated with the grain sand size distribution observed in Figure S4a [39] are not detected.

The electrostatic and Van der Waals forces are described by the Derjaguin, Landau, Verwey and Overbeek (DLVO) theory [45, 46] and have been studied extensively in laboratory experiments [47-50]. When the surfaces of the precipitates and mineral grains are oppositely charged, electrostatic and Van der Waals forces strongly attach the particles to the mineral grain surface [51, 52]. When the surfaces of the precipitates and mineral grains have the same effective surface charge, short range electrostatic repulsion acts as a barrier to chemisorption and the travelling particles will only be weakly bound by van der Waals attraction [51, 52]. The effective surface charge is given by the Z_p of the precipitates (Z_p). The Z_p reported for the U^{VI} precipitates (Table 1) at pH 10.5 and 11.5 is -22.4±1.04 mV and -20.9±0.19 mV while the Z_p for the quartz sand (Table S1) at pH 10.5 and pH 11.5 is -40.8±1.19 mV and -42.0±2.16 mV. This means there will be an energy barrier to chemical attachment of the U^{VI} precipitates to the quartz mineral surface. This is evidenced by previous work [14] in which U^{VI} was not removed on the quartz surface during end over end rotating batch experiments, where the high solution to solid ratio prevents physical entrapment of U^{VI} precipitates. Therefore, it is unlikely that chemical attachment of U^{VI} to the quartz sand surface is occurring.

Further evidence supporting physical immobilisation is provided by the retention profiles presenting in Figure 6. Attachment processes which includes the transport of particles to a porous media surface, and subsequent chemical attachment is modelled as a first order reaction. Therefore the U^{VI} concentration

would be expected to decrease exponentially throughout the length of the column [44]. However, the precipitates should be immobilised near the column inlet when influenced by significant particle straining [44]. At pH 11.5, virtually all U^{VI} is immobilised near the inlet, with retention profiles similar to those observed in particle straining experiments by Bradford and co-workers [44]. At pH 10.5, there is clearly increased removal near the column inlet as seen during the pH 11.5 experiments, however, U^{VI} is immobilised throughout the length of the column, which could reflect the smaller diameter of the precipitates at pH 10.5 and subsequent penetration into the column, as well as continued U^{VI} precipitation and subsequent physical immobilisation during transport through the quartz sand.

Conclusions

The aim of this study was to characterise experimentally the effect of pH on U^{VI} removal and particle formation in alkaline sodium solutions and to assess subsequent transport through quartz sand within the pH window of 10.5 and 12.5.

Static batch experiments showed significant control of the pH on the amount of U^{VI} removed. After 48 hours, 73 to 85% and 89 to 96% of U^{VI} were removed from the solution at pH 10.5 and 11.5, respectively, through the formation of particles. In situ size measurements indicated the particles had a hydrodynamic diameter of 640±111 nm and 837±142 nm with Z_p -22.4±1.04 and -20.9±0.19 mV at pH 10.5 and pH 11.5, respectively. XRD indicated U^{VI} precipitates as clarkeite and studtite. We did not find significant formation of U^{VI} particles ≥0.2 µm diameter at pH 12.5.

All the U^{VI} containing particles at pH 11.5 were immobilised within 1.5 cm of the column inlet. The effective surface charge for the U^{VI} particles and the quartz surface were both negative providing a first indication that there was a barrier to attachment. The d_p/d_{50} ratio indicate significant particle straining will be occurring in the columns. Therefore, immobilisation of the U^{VI} particles is attributed to the physical

properties of the U^{VI} particles and quartz sand. Up to 19% of U^{VI} eluted from the columns in particulate form with diameter ≥0.2 μm which may reflect the smaller diameter of the precipitates formed at pH 10.5.

Our results imply that in alkaline sodium solutions with pH ranging between 10.5 and 11.5, U^{VI} will be immobilised in porous media, even though chemical interactions between the U^{VI} precipitates and quartz surface are unfavourable. This highlights that current conceptual models based solely on sorption processes need to consider immobilisation of U^{VI} due to the physical properties of the precipitates and porous media.

Credit Author Statement

Conceptualization: Kirby, Weiss, Krevor

Data curation: Kirby, Weiss, Kenney, Watson, Najorka

Formal analysis: Kirby, Weiss, Kenney, Watson, Najorka

Funding acquisition: Weiss, Krevor

Investigation: Kirby, Weiss, Krevor

Methodology: Kirby, Weiss, Krevor Project administration: Kirby, Weiss, Krevor Resources: Kirby, Weiss, Krevor

Software: Kirby, Weiss, Krevor

Supervision: Kirby, Weiss, Krevor

Validation: Kirby, Weiss, Krevor, Watson, Najorka

Visualization: Kirby, Weiss, Krevor

Roles/Writing - original draft: Kirby, Weiss, Krevor, Kenney, Watson, Najorka

Writing - review & editing: Kirby, Weiss, Krevor, Kenney, Watson, Najorka

Declaration of interests

The authors declare that they have no known competing financial interests or personal relationships that could have appeared to influence the work reported in this paper.

Acknowledgements

We acknowledge the Natural Environment Research Council, Radioactive Waste Management Limited, and Environment Agency for the funding received for this project through the Radioactivity and the Environment (RATE) programme. We thank Dr Simon Norris from RWM and Dr Gavin Thomson for their insights in writing this manuscript.

Figures

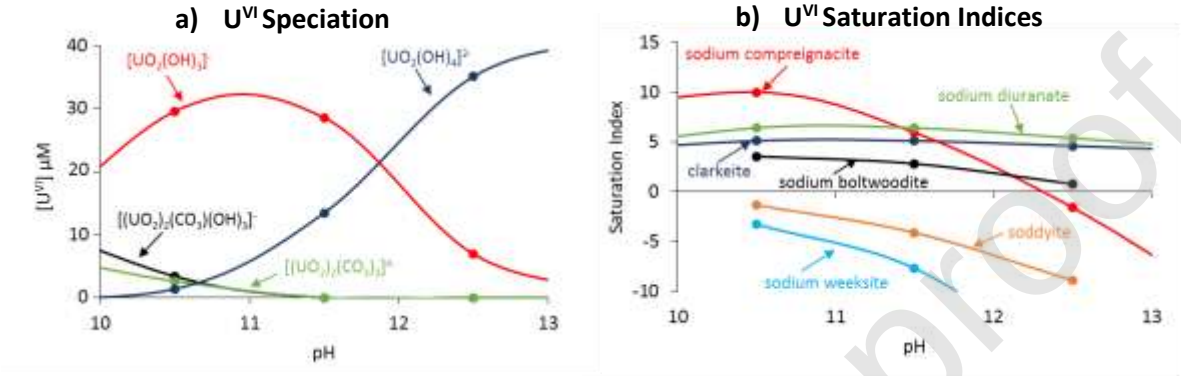

Figure 1. Plot a) shows the calculated concentrations of different U^{VI} species. Plot b) provides saturation indices for sodium compreignacite ($Na_2(UO_2)_6O_4(OH)_6 \bullet 7H_2O$), sodium diuranate ($Na_2U_2O_7$), clarkeite ($NaUO_2O(OH)$), sodium boltwoodite ($Na(H_3O)(UO_2)(SiO_4) \bullet H_2O$), sodium weeksite ($Na_2(UO_2)_2(Si_2O_5)_3 \bullet 4H_2O$) and soddyite ($(UO_2)_2SiO_4 \bullet 2H_2O$). The chemical conditions are [U^{VI}] = 42 µM, [NaCl] = 0.1 M, Σ[CO_2] = 220 µM, [O_2] in equilibrium with the atmosphere. The [Si] is 1.44, 2.38 and 0.95 ppm at pH 10.5, pH 11.5 and pH 12.5 respectively. The [Si] represents the concentration eluting from the quartz sand columns.

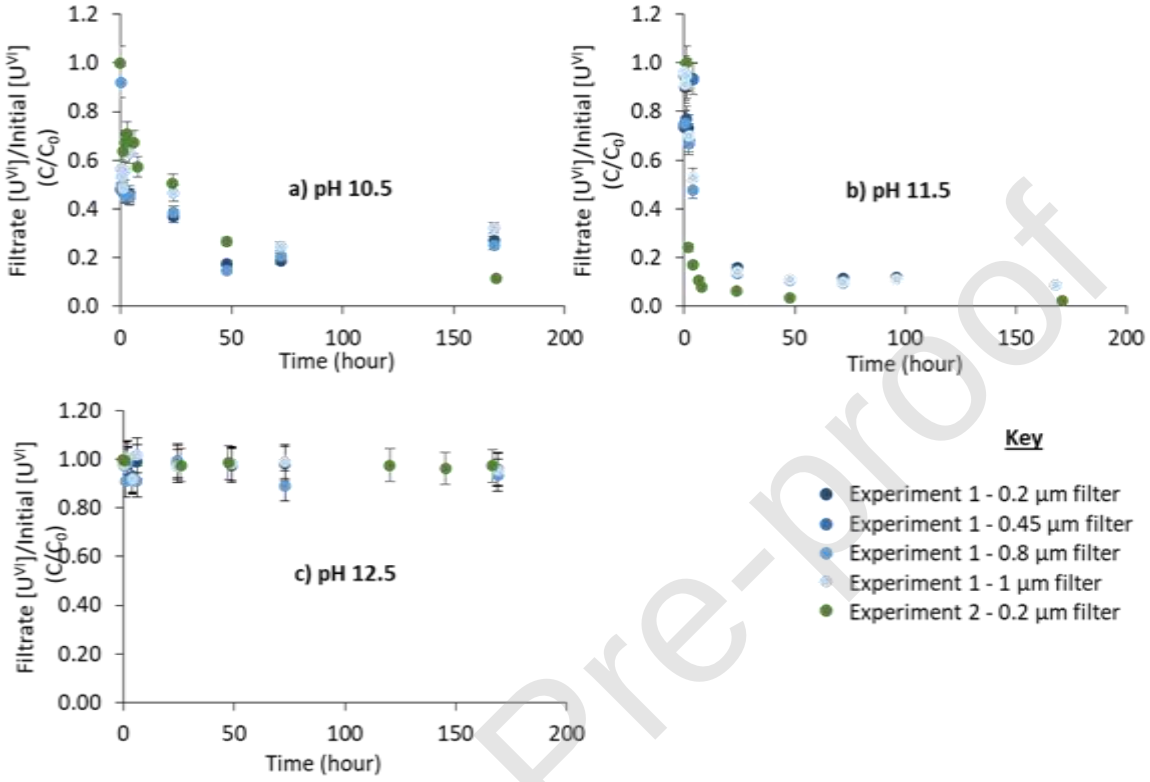

Figure 2. Static batch experiments at a) pH 10.5, b) pH 11.5 and c) pH.12.5 for 10 ppm UVI, 0.1 M NaCl solutions. The blue and green data points represent the two repeat experiments. The darkest and lightest shade of blue represent the smallest (0.2 µm) and largest (1 µm) nylon filter membrane pore size. The green data points represent samples filtered through 0.2 µm pore size nylon filter membranes. The typical error of concentration data after error propagation was ± 7%.

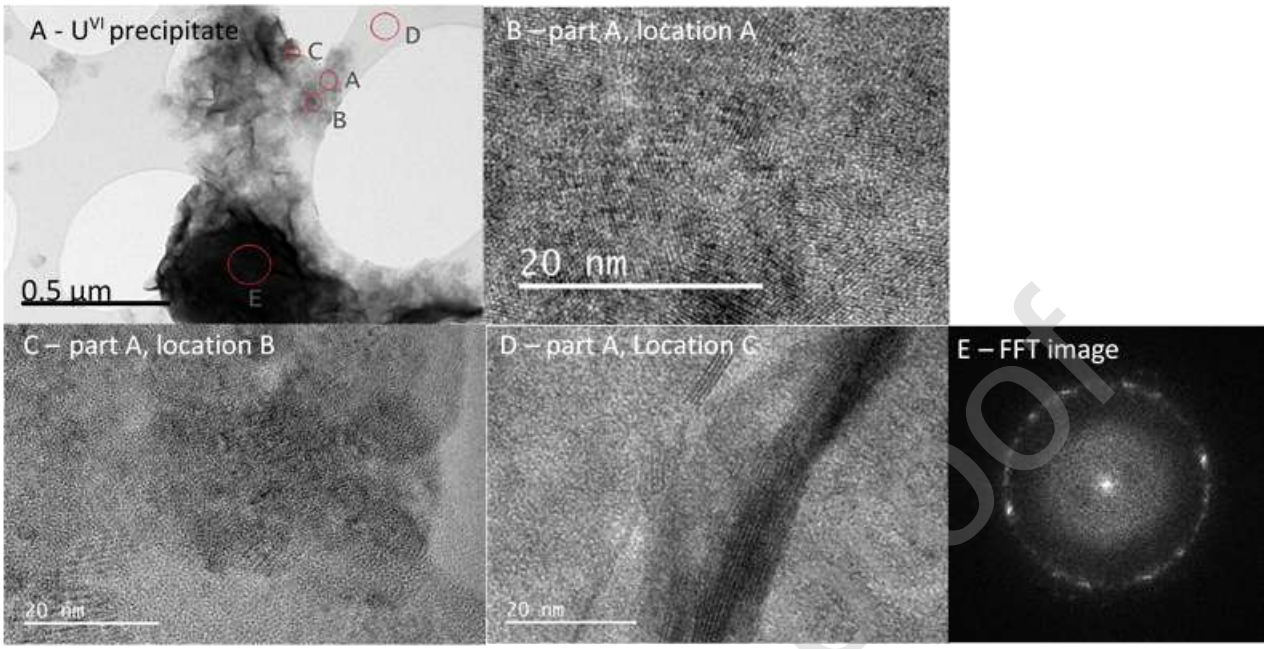

Figure 3. TEM images of the U^{VI} precipitates from an initially 42 µM UVI, 0.1M NaCl pH 10.5 solution. Panel A is at 8k magnification. Panels B, C and D were imaged at 400k magnification and represents Location A, B and C circled on panel A. Panel E is a Fast Fourier Transform image of the precipitate. Panels A and D have been presented as part of a previous study in our group [14].

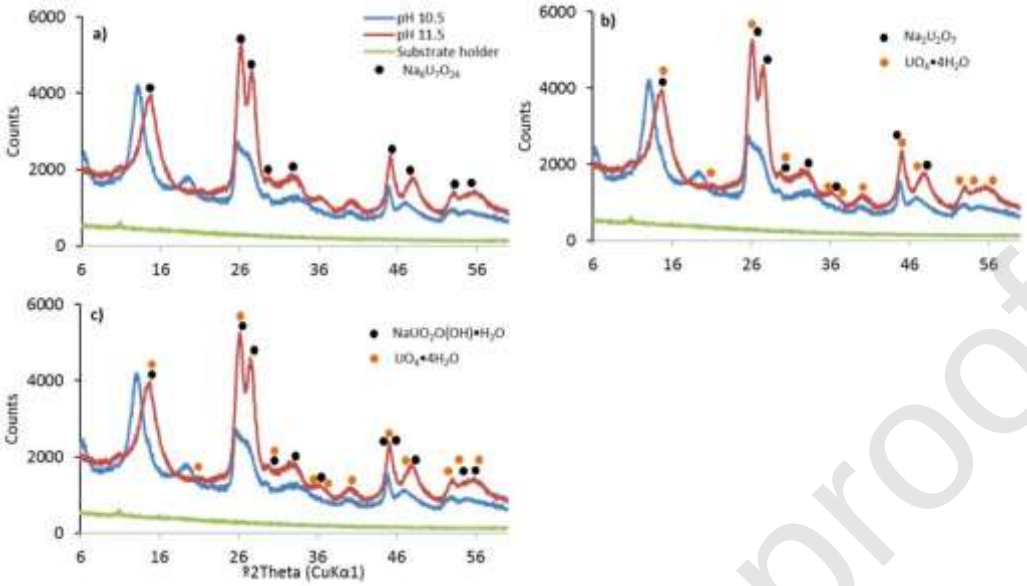

Figure 4. X-ray diffractograms of the U^{VI} containing solids >0.2 micron precipitated from solutions of 10 mg/L U^{VI}, 0.1 M NaCl originally prepared at pH 10.5 (blue) and pH 11.5 (red). The green diffractogram represents the sapphire substrate holder. Part a) contains the reference pattern for sodium diuranate $Na_6U_7O_{24}$ (black circles). Part b) contains the reference pattern for sodium diuranate ($Na_2U_2O_7$) and studtite ($UO_4•4H_2O$) as black and orange circles respectively. Part c) contains the reference pattern for clarkeite ($NaUO_2O(OH)•H_2O$) and studtite as black and orange circles respectively.

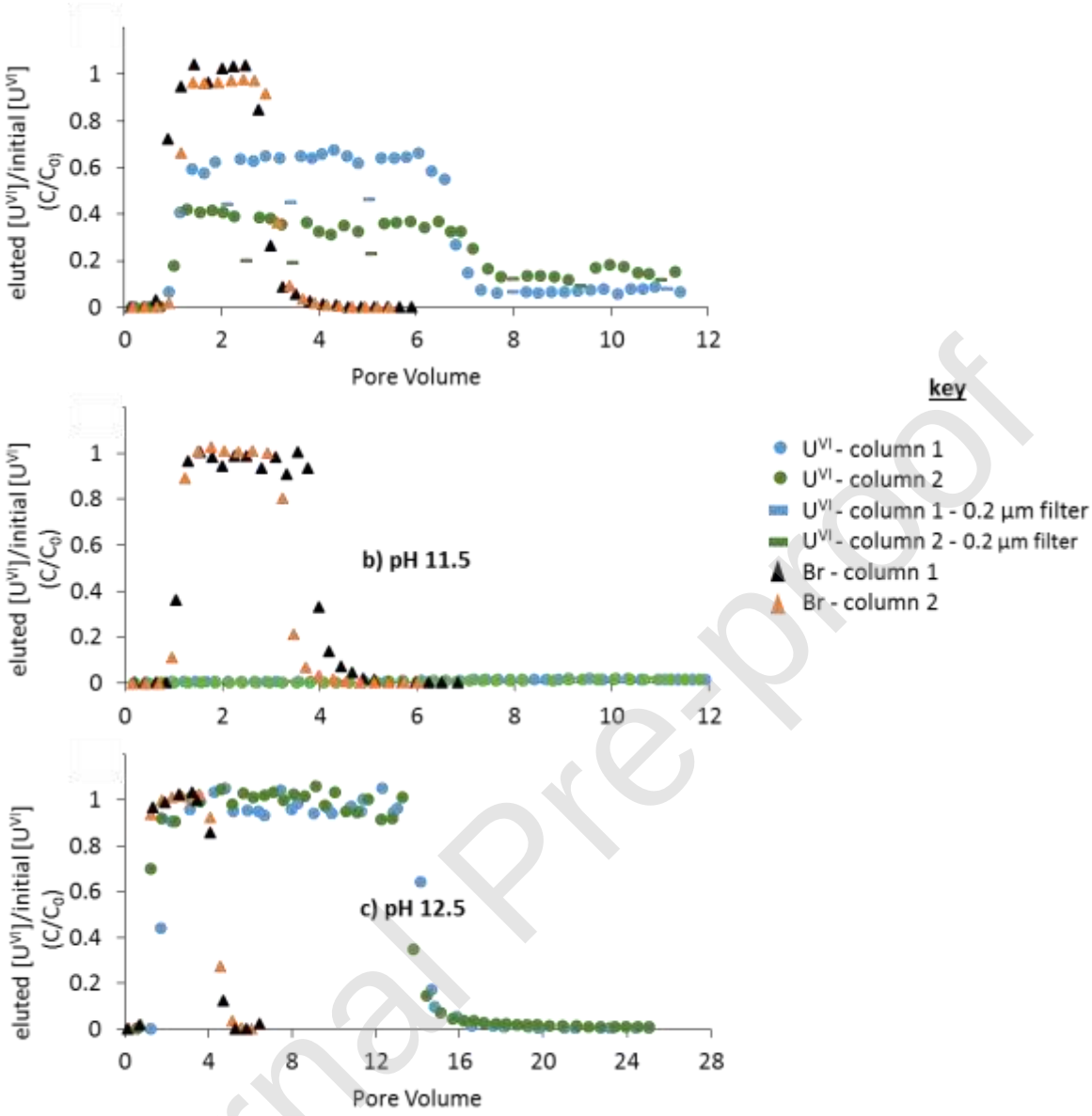

Figure 5. The elution curves of U^{VI} at a) pH 10.5, b) pH 11.5 and c) pH 12.5. The ratio of the measured U^{VI} outlet concentration/initial U^{VI} concentration is provided on the Y-axis. The ICP-MS error is ±7%. The first and second columns data points are blue and green. The dashes on the elution curves are the ratio of U^{VI} concentration in the filtrate/initial U^{VI} concentration for samples filtered through 0.2 µm pore size nylon filter membranes. The Br non-reactive tracer is included as black and orange triangles for the first and second column experiments respectively.

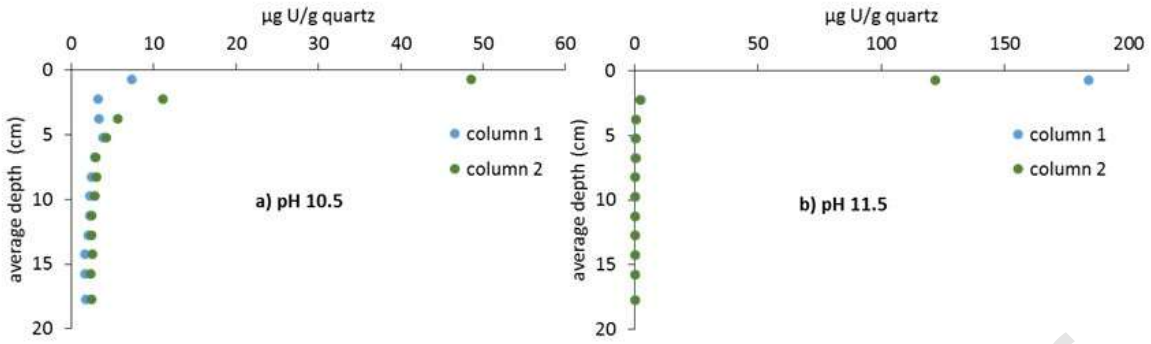

Figure 6. The retention profiles of U^{VI} at a) pH 10.5 and b) pH 11.5 for the first (blue) and second (green) column experiments respectively. The mass of U^{VI} immobilised in each depth increment has been normalised against the mass of quartz sand collected in that increment.

Tables

Experiment	pH	Size– intensity (nm)	Size- Z average (nm)	PDI	Z_p (mV)
pH 10.5 – 1	10.34	666±113	785±94	1.000	-23.5±0.67
pH 10.5 – 2	10.34	664±114	786±113	1.000	-23.0±0.75
pH 10.5 – 3	10.35	618±106	707±40	1.000	-20.6±1.70
pH 10.5 –	10.34	640±111	759±82	1.000	-22.4±1.04
pH 11.5 – 1	11.40	860±154	1139±128	1.000	-20.0±1.22
pH 11.5 – 2	11.43	765±124	988±101	1.000	-22.1±0.96
pH 11.5 – 3	11.43	885±149	1386±264	1.000	-20.5±0.84
pH 11.5 –	11.42	837±142	1171±164	1.000	-20.9±0.19
pH 12.5 – 1	12.43	No particles detected		-	-
pH 12.5 – 2	12.47			-	-

Table 1. The particle diameter (nm) and zeta potential (Zp) measurements of the U^{VI} precipitates at 25˚C. The size at the maximum peak height is provided along with the cumulative frequency size (Z-average) and corresponding polydispersity index (PDI). The error is one S.D. of three or more measurement points. The limit of detection of the particle size was 200 nm

Experiment	ρ_b (g/cm^3)	PV (ml)	Φ	Q (cm^3/min)	q (cm/min)	v (cm/min)
pH 10.5-R1	1.60	11.09	0.45	0.45±0.02	0.34±0.02	0.76±0.04
pH 10.5-R2	1.60	10.77	0.44	0.45±0.03	0.34±0.02	0.77±0.05
pH 11.5-R1	1.68	11.10	0.45	0.53±0.04	0.39±0.03	0.88±0.07
pH 11.5-R2	1.62	10.69	0.43	0.47±0.02	0.36±0.02	0.83±0.04
pH 12.5-R1	1.59	7.86	0.31	0.52±0.09	0.39±0.06	1.25±0.21
pH 12.5-R2	1.59	8.78	0.35	0.53±0.12	0.40±0.09	1.13±0.25

Table 2. The physical properties of the quartz sand columns. The parameters provided are the dry bulk density (ρ_b), pore volume (PV), porosity (ϕ), flow rate (Q), darcy velocity (q) and average linear velocity (v). The error provided for Q, q and v is one S.D. of ≥10 measurements during U^{VI} injection.

Experiment	pH_{inlet}	pH_{outlet}	$[Si]_{inlet}$ (ppm)	$[Si]_{outlet}$ no U^{VI} (ppm)	$[Si]_{outlet}$ U^{VI} (ppm)
pH 10.5 – R1	10.32-10.55	10.07-10.37	0.40-0.47	1.23±0.42	1.44±0.27
pH 10.5 – R2	10.26-10.54	10.04-10.36	0.28-0.58	0.94	1.11
pH 11.5 – R1	11.43-11.47	11.39-11.40	0.28-0.30	2.38±0.73	1.17±0.25
pH 11.5 – R2	11.37-11.49	11.26-11.40	0.46-0.53	1.19	2.20
pH 12.5 – R1	12.40-12.47	12.30-12.45	<0.29	-	0.95±0.02
pH 12.5 – R2	12.40-12.47	12.33-12.46	<0.29	-	0.95±0.02

Table 3. The pH and [Si] (given in ppm) measured during the column experiments. The pH was measured in the column inlet solution (pH inlet) and samples collected at the outlet (pH outlet). The [Si] was measured in the inlet solutions ([Si] inlet) and in samples collected at the outlet before U^{VI} injection ([Si] outlet no U^{VI}) and during U^{VI} injection ([Si] outlet U^{VI}). The error reported for [Si] are one S.D. of three samples. [Si] data without errors are obtained from one sample. The standard error for pH was typically ± 0.05 pH units.

Experiment	%U in filtrate of inlet solution at start	%U in filtrate of inlet solution at end	%U eluted during U injection	%U filtered at outlet during U injection	%U eluted during U-free injection	%U filtered at outlet during U-free injection	%U recovery
pH 10.5 – 1	60 (0.2 µm filter) 55 (0.45 µm filter) 55 (1 µm filter)	55 (0.2 µm filter) 57 (0.45 µm filter) 54 (1 µm filter)	64±2	45±1	7±0.9	6.4±0.2	86
pH 10.5 - 2	35 (0.2 µm filter) 34 (0.45 µm filter) 46 (1 µm filter)	38 (0.2 µm filter) 37 (0.45 µm filter) 44 (1 µm filter)	37±3	21±2	15±2	11±2	90
pH 11.5 - 1	2.5 (0.2 µm filter) 2.6 (0.45 µm filter) 3.3 (1 µm filter)	2.3 (0.2 µm filter) 2.4 (0.45 µm filter) 2.5 (1 µm filter)	0.9±0.3	0.8±0.05	1.6±0.2	1.7±0.2	91
pH 11.5 - 2	2.4 (0.2 µm filter) 2.5 (0.45 µm filter) 2.3 (1 µm filter)	2.6 (0.2 µm filter) 2.6 (0.45 µm filter) 2.6 (1 µm filter)	0.3±0.2	0.3±0.06	1.4±0.3	1.5±0.05	74

Table 4. Details on the amounts of U^{VI} remaining in solution, including the %U in the filtrate in the input solution, the %U eluted from the column, %U in filtrate after solution collected at the column outlet was filtered through a 0.2 µm filter membrane, and the total %U recovered following sand clean

References

[1] DECC, Implementing geological disposal: A framework for the long term management of higher activity radioactive waste, Department of Energy and Climate Change, London, SW1A 2AW, 2014, p. 55.

[2] SG, Implementation strategy for Scotland's policy on higher activity radioactive waste, Scottish Government, Edinburgh, EH1 3DG, 2016, p. 46.

[3] LLWR, Engineering Design, The 2011 Environmental Safety Case, Cumbria, CA19 1XH, 2011, p. 115.

[4] W.R. Alexander, R. Dayal, K. Eagleson, J. Eikenberg, E. Hamilton, C.M. Linklater, I.G. McKinley, C.J. Tweed, A natural analog of high pH cement pore waters from the Maqarin area of northern Jordan. 2. Results of predictive geochemical caluclations, Journal of Geochemical Exploration 46(1) (1992) 133-146.

[5] H.N. Khoury, E. Salameh, I.D. Clark, P. Fritz, W. Bajjali, A.E. Milodowski, M.R. Cave, W.R. Alexander, A natural analog of high pH cement pore waters from the Maqarin area of northern Jordan.1. Introduction to the site, Journal of Geochemical Exploration 46(1) (1992) 117-132.

[6] A. Rizoulis, A.E. Milodowski, K. Morris, J.R. Lloyd, Bacterial Diversity in the Hyperalkaline Allas Springs (Cyprus), a Natural Analogue for Cementitious Radioactive Waste Repository, Geomicrobiology Journal 33(2) (2016) 73-84.

[7] R.E. Gephart, A short history of waste management at the Hanford Site, Physics and Chemistry of the Earth 35(6-8) (2010) 298-306.

[8] S.A. Parry, L. O'Brien, A.S. Fellerman, C.J. Eaves, N.B. Milestone, N.D. Bryan, F.R. Livens, Plutonium behaviour in nuclear fuel storage pond effluents, Energy & Environmental Science 4(4) (2011) 1457-1464.

[9] J.E. Szecsody, M.J. Truex, N.P. Qafoku, D.M. Wellman, T. Resch, L.R. Zhong, Influence of acidic and alkaline waste solution properties on uranium migration in subsurface sediments, Journal of Contaminant Hydrology 151 (2013) 155-175.

[10] D.I. Kaplan, T.L. Gervais, K.M. Krupka, Uranium(VI) sorption to sediments under high pH and ionic strength conditions, Radiochimica Acta 80(4) (1998) 201-211.

[11] Q.H. Fan, L.M. Hao, C.L. Wang, Z. Zheng, C.L. Liu, W.S. Wu, The adsorption behavior of U(VI) on granite, Environmental Science-Processes & Impacts 16(3) (2014) 534-541.

[12] Y.Y. Zhang, H.G. Zhao, Q.H. Fan, X.B. Zheng, P. Li, S.P. Liu, W.S. Wu, Sorption of U(VI) onto a decarbonated calcareous soil, Journal of Radioanalytical and Nuclear Chemistry 288(2) (2011) 395-404.

[13] J.P.L. Kenney, T. Ellis, F.S. Nicol, A.E. Porter, D.J. Weiss, The effect of bacterial growth phase and culture concentration on U(VI) removal from aqueous solution, Chemical Geology 482 (2018) 61-71.

[14] J.P.L. Kenney, M.E. Kirby, J. Cuadros, D.J. Weiss, A conceptual model to predict uranium removal from aqueous solutions in water-rock systems associated with low- and intermediate-level radioactive waste disposal, RSC Advances 7(13) (2017) 7876-7884.

[15] P. Bots, K. Morris, R. Hibberd, G.T.W. Law, J.F.W. Mosselmans, A.P. Brown, J. Doutch, A.J. Smith, S. Shaw, Formation of stable uranium(VI) colloidal nanoparticles in conditions relevant to radioactive waste disposal, Langmuir 30(48) (2014) 14396-14405.
[16] W.X. Ding, J.A. Botha, B.C. Hanson, I.T. Burke, Aqueous hydroxylation mediated synthesis of crystalline calcium uranate particles, Journal of Alloys and Compounds 688 (2016) 260-269.
[17] N.A. Wall, S.B. Clark, J.L. McHale, Synthesis and characterization of 1:1 layered uranyl silicate mineral phases, Chemical Geology 274(3-4) (2010) 149-157.
[18] M. Altmaier, E. Yalcintas, X. Gaona, V. Neck, R. Muller, M. Schlieker, T. Fanghanel, Solubility of U(VI) in chloride solutions. I. The stable oxides/hydroxides in NaCl systems, solubility products, hydrolysis constants and SIT coefficients, Journal of Chemical Thermodynamics 114 (2017) 2-13.
[19] T. Yamamura, A. Kitamura, A. Fukui, S. Nishikawa, T. Yamamoto, H. Moriyama, Solubility of U(VI) in highly basic solutions, Radiochimica Acta 83(3) (1998) 139-146.
[20] E.S. Ilton, C. Liu, W. Yantasee, Z. Wang, D.A. Moore, A.R. Felmy, J.M. Zachara, The dissolution of synthetic Na-boltwoodite in sodium carbonate solutions, Geochimica et Cosmochimica Acta 70(19) (2006) 4836-4849.
[21] B. Uyusur, C.Y. Li, P.C. Baveye, C.J.G. Darnault, pH-dependent reactive transport of uranium(VI) in unsaturated sand, Journal of Soils and Sediments 15(3) (2015) 634-647.
[22] H. Moll, A. Rossberg, R. Steudtner, B. Drobot, K. Müller, S. Tsushima, Uranium(VI) Chemistry in Strong Alkaline Solution: Speciation and Oxygen Exchange Mechanism, Inorganic Chemistry 53(3) (2014) 1585-1593.
[23] S.P. Xu, B. Gao, J.E. Saiers, Straining of colloidal particles in saturated porous media, Water Resources Research 42(12) (2006).
[24] J. Stetefeld, S. McKenna, T. Patel, Dynamic light scattering: a practical guide and applications in biomedical sciences, Biophysical Reviews 8(4) (2016) 409-427.
[25] A.V. Delgado, F. Gonzalez-Caballero, R.J. Hunter, L.K. Koopal, J. Lyklema, Measurement and interpretation of electrokinetic phenomena, Journal of Colloid and Interface Science 309(2) (2007) 194-224.
[26] A. Kern, W. Eysel, Mineralogisch-Petrograph. Inst., Univ. Heidelberg, Germany ICDD Grant-in-Aid, 1993.
[27] Avizo, Avizo, https://www.fei.com/software/amira-avizo/, 2016.
[28] H. Dong, M.J. Blunt, Pore-network extraction from micro-computerized-tomography images, Physical Review E 80(3) (2009).
[29] C.V. Chrysikopoulos, A.F. Aravantinou, Virus inactivation in the presence of quartz sand under static and dynamic batch conditions at different temperatures, Journal of Hazardous Materials 233-234 (2012) 148-157.
[30] D.J. Weiss, K. Boye, C. Caldelas, S. Fendorf, Zinc isotope fractionation during early dissolution of biotite granite, Soil Science Society of America Journal 78(1) (2014) 171-179.
[31] S.A. Bradford, J. Simunek, M. Bettahar, M.T. Van Genuchten, S.R. Yates, Modeling colloid attachment, straining, and exclusion in saturated porous media, Environmental Science & Technology 37(10) (2003) 2242-2250.
[32] D.L. Parkhurst, C.A.J. Appelo, Description of input and examples for PHREEQC version 3--A computer program for speciation, batch-reaction, one-dimensional transport, and inverse geochemical calculations, U.S. Geological Survey Techniques and Methods, Book 6, U.S. Geological Survey2013, p. 497.

[33] E. Giffaut, M. Grive, P. Blanc, P. Vieillard, E. Colas, H. Gailhanou, S. Gaboreau, N. Marty, B. Made, L. Duro, Andra thermodynamic database for performance assessment: ThermoChimie, Applied Geochemistry 49 (2014) 225-236.
[34] R. Guillaumont, Fanghänel T, J. Fuger, I. Grenthe, N. V., D.A. Palmer, M.H. Rand, Update on the Chemical Thermodynamics of Uranium, Neptunium, Plutonium, Americium and Technetium, NEA OECD, North-Holland, Amsterdam, 2003.
[35] C.A. Wamser, J. Belle, E. Bernsohn, B. Williamson, The Constitution of the Uranates of Sodium1, Journal of the American Chemical Society 74(4) (1952) 1020-1022.
[36] L.M. Kovba, Sodium Diuranate Crystal Structure, Soviet Radiochemistry 14 (1972) 727-730.
[37] J. Cejka, J. Sejkora, M. Deliens, New data on studtite, UO4 center dot 4H(2)O, from Shinkolobwe, Shaba, Zaire, Neues Jahrbuch Fur Mineralogie-Monatshefte (3) (1996) 125-134.
[38] R.J. Finch, R.C. Ewing, Clarkeite: New chemical and structural data, American Mineralogist 82(5-6) (1997) 607-619.
[39] P.H. Nelson, Pore-throat sizes in sandstones, tight sandstones, and shales, Aapg Bulletin 93(3) (2009) 329-340.
[40] C.P. Romero, R.I. Jeldres, G.R. Quezada, F. Concha, P.G. Toledo, Zeta potential and viscosity of colloidal silica suspensions: Effect of seawater salts, pH, flocculant, and shear rate, Colloids and Surfaces a-Physicochemical and Engineering Aspects 538 (2018) 210-218.
[41] M.L. Brusseau, Transport of reactive contaminants in hetergeneous prous media, Reviews of Geophysics 32(3) (1994) 285-313.
[42] J.J. De Yoreo, P.G. Vekilov, Principles of crystal nucleation and growth, Biomineralization 54 (2003) 57-93.
[43] K.W. Kolasinski, Physical Chemistry: How Chemistry Works, United Kingdom: John Wiley & Sons Inc2016.
[44] S.A. Bradford, S.R. Yates, M. Bettahar, J. Simunek, Physical factors affecting the transport and fate of colloids in saturated porous media, Water Resources Research 38(12) (2002).
[45] B. Derjaguin, L. Landau, Theory of the stability of strongly charged lyophobic sols and of the adhesion of strongly charged particles in solutions of electrolytes, Acta Physicochimica U. S. S. R 14 (1941) 733 –762.
[46] E.J.W. Verwey, O. TH.G., Theory of the stability of lyophobic colloids, Elsevier, Amsterdam, 1948.
[47] X.Q. Li, P.F. Zhang, C.L. Lin, W.P. Johnson, Role of hydrodynamic drag on microsphere deposition and re-entrainment in porous media under unfavorable conditions, Environmental Science & Technology 39(11) (2005) 4012-4020.
[48] M. Elimelech, M. Nagai, C.H. Ko, J.N. Ryan, Relative insignificance of mineral grain zeta potential to colloid transport in geochemically heterogeneous porous media, Environmental Science & Technology 34(11) (2000) 2143-2148.
[49] X.Q. Li, T.D. Scheibe, W.P. Johnson, Apparent decreases in colloid deposition rate coefficients with distance of transport under unfavorable deposition conditions: A general phenomenon, Environmental Science & Technology 38(21) (2004) 5616-5625.
[50] M. Elimelech, C.R. Omelia, Kinetcis of colloid particles in porous media, Environmental Science & Technology 24(10) (1990) 1528-1536.
[51] J.N. Ryan, M. Elimelech, Colloid mobilization and transport in groundwater, Colloids and Surfaces a-Physicochemical and Engineering Aspects 107 (1996) 1-56.

[52] I.L. Molnar, W.P. Johnson, J.I. Gerhard, C.S. Willson, D.M. O'Carroll, Predicting colloid transport through saturated porous media: A critical review, Water Resources Research 51(9) (2015) 6804-6845.